Chapter 1

Global Dynamics and Fast Indicators

Carles Simó
Dept. de Matemàtica Aplicada i Anàlisi, Univ. de Barcelona, Gran Via, 585, Barcelona 08007, Spain

Dynamical systems play an important role in understanding many problems in science. The variety of difficulties that they present to the dynamicist is huge. Local problems around some well known object (a point, a periodic or quasi-periodic orbit, an invariant manifold, etc) can be studied by different methods. A combination of analytic, geometric and topological tools provides a detailed account of this local dynamics and the bifurcations which occur when changing parameters. On the other hand, more global problems, facing to a big part of the phase space or to a large set in the parameter space, can be studied by using probabilistic methods and by computing several numeric indicators.

But it can happen that we would like to combine both things: a relatively detailed knowledge of the dynamics in a large set. To this end it is useful

- to extend the local analysis to larger domains, say by using normal forms up to some relatively large order, so that they can give good quantitative information. Unfolding of the bifurcations found. This analysis provides a guidance to the numeric experiments to be done,
- to do systematic numeric experiments, like computation of invariant objects: fixed points, periodic orbits, tori, etc, and, if it applies, the related stable, unstable and centre manifolds. Intersections of the

manifolds (homoclinic and heteroclinic phenomena) and quantitative measures associated to them. Continuation of these objects with respect to parameters and detection and analysis of the bifurcations. These experiments, in turn, give hints on new phenomena to be investigated.

This programme has been carried out previously in several cases, like [3, 13], [5], [6], [7], [14], [12].

However, both approaches can require an important effort. It is suitable to have *fast indicators* aiming at a significant knowledge of the dynamics in a quick way (with the help of arrays of processors). Both the design of the indicators and the interpretation of the results must be guided by

- the known dynamical phenomena on the considered class of systems,
- the role of the numerical errors,
- computational efficiency.

In this paper we sketch some tools. They are presented by showing how they apply to some examples, restricting to conservative systems, and summarizing part of the results. But are described with generality enough so that they can be used in many other problems in "experimental" mathematics.

1.1 A model problem in $1\frac{1}{2}$ degrees of freedom

Consider a periodically perturbed pendulum with differential equation

$$x'' = (\alpha + \beta \cos t) \sin x \, . \tag{1.1}$$

This problem has received a strong attention because it is one of the simplest paradigms showing most of the dynamics in his class. For motivation and recent results see [11] and, in a slightly different context (limit of two coupled pendulums) see [9]. A part of the methods of the present paper are used in [2].

It is convenient to introduce $y = x'$. The study can be done by means of the "time the period map" $P_{\alpha,\beta}(x,y) = \varphi(2\pi; 0, x, y; \alpha, \beta)$, an area preserving map. In what follows we shall denote it simply as P. The variable $x \in \mathbb{S}^1$, but it is also useful to look at x on the lift (e.g., to distinguish different fixed points of P.) For $\beta = 0$ the invariant curves of P coincide with the orbits of a pendulum.

The symmetries of (1.1) imply that it is enough to consider both parameters $\alpha, \beta \geq 0$. The dynamics is also symmetric (reversible) with respect to both the x and y axes, that is $P^{-1}S_x = S_xP$, $P^{-1}S_y = S_yP$, where S_x, S_y are the symmetries with respect the x and y axes.

It is clear that for $\alpha, \beta << 1$ and y small we have a "slow pendulum" with a fast time-periodic perturbation. In this region the problem is suitable for the use of normal forms (see [11]). On the other hand, for (α, β)

fixed and y sufficiently large, the fast angle is x and t plays the slow role. A similar thing happens if $1 << \beta < \gamma\alpha$ with γ bounded away from 1, except in a "neighbourhood of the separatrix", where the two dynamics (the frozen pendulum and the perturbation) are comparable.

This suggests that for any (α, β) most of the interesting dynamics occurs in a region without rotational invariant curves (i.e., curves not crossing $y = 0$, being a graph over $\mathbb{S}^1$, *ric* from now on.) Outside this region most of the points belong to a *ric*. The width of the chaotic regions becomes exponentially small with respect to $|y|$.

1.2 Bounding the region of interest

To bound the *domain of interest* (from now on DI) we can look for a *ric* close enough to the upper boundary of the domain. We shall refer loosely to this curve as y_{min}. To identify such a curve we can use either the values $y_{min}(x = 0)$, $y_{min}(x = \pi)$ or the rotation number of P restricted to it, $\rho_{y_{min}}$. The three values are worth to be considered. We intend to see their evolution as (α, β) change. An exploration of this kind, with a similar algorithm, has been used in [15].

With our loose definition the curve (say, the "first" curve) is not uniquely determined. It depends on the algorithm and its implementation. Hopefully this affects mildly the value of, say, $y_{min}(x = \pi)$.

1.2.1 The algorithm

Given (α, β) we look for the value of $y_{min}(x = 0)$. Due to the symmetry one has $S_y(y_{min}) = y_{min}$. We scan the y axis searching for $y_{min}(x = 0)$. To solve equation (1.1) it is convenient to use an accurate and fast method. We have adopted a Taylor series method (see Appendix).

The steps of the algorithm are as follows:

- For a given initial point $Q_0 = (0, y_0), y_0 > 0$, we proceed to compute iterates under P. We transport also an initial "random" vector (e.g. $v_0 = (1, 0)$) under the differential DP by integration of the variational equations. In this way points $Q_k = P^k(Q_0) = (x_k, y_k)$, with $x_k \in [0, 2\pi)$, and vectors $v_k = DP^k(Q_0)v_0$ are obtained, up to a maximum of N iterates. We also keep track of the value of x_k on the lift, $\hat{x}_k$. Let $\Delta_k = \hat{x}_k - \hat{x}_{k-1}$. We compute the values $\Delta_{min} = \min_{j=1,\dots,k} \Delta_j$ and $\Delta_{max} = \max_{j=1,\dots,k} \Delta_j$.
- We discard the current initial value, y_0, as soon as some $y_k \leq 0$, $k \leq N$. Then y_0 is incremented by δ_{y_0} and the process starts again.
- If $|v_k| > L_{max}$ for some fixed value of L_{max} and $k \leq N$ we discard also y_0 and proceed as before.
- If $\Delta_k \leq 0$ or $\Delta_{max} - \Delta_{min} \geq 2\pi$ for some $k \leq N$ we discard y_0 as before.

- Every n iterates we sort the points Q_k, $k = 0, \dots, mn$ for $m \in \mathbb{N}$ by increasing order of x_k. Due to the symmetry we also use the preimages $Q_{-k} = (-x_k, y_k)$. We check for the slope associated to points with nearby x values and discard the y_0 value if the slope exceeds some S_{max} (which depends on (α, β).) Care must be taken to not to use too close values of x, due to the effect of numeric errors.
- If three consecutive (after ordering) values of x correspond to iterates numbers k_1, k_2 and k_3, let $l = k_2 - k_1$. Then one must have $k_3 = k_3^t := k_2 + l$, unless $k_3^t \notin J = [-nm, nm]$ or, in case $k_3^t \in J$, if $k_3 - l \notin J$. Otherwise we discard y_0 and proceed as before.
- A "number of revolutions" on $\mathbb{S}^1$, $n(k)$, can be assigned to every Q_k as follows. Let $n_0 = 0$. For $j > 0$ we put $n(j) = n(j-1)$ if $x_j > x_{j-1}$ (in $[0, 2\pi)$.) Otherwise $n(j) = n(j-1) + 1$. In a similar way we put $n(-j) = -n(j) - 1$.
  Then it is possible to produce upper and lower estimates of the rotation number (on $\mathbb{S}^1$), assuming that the points are on a *ric*, as follows. Let l_j be the number of the iterate which has the x component in the jth place when it is sorted. Let $q_j = (n(l_{j+1}) - n(l_j))/(l_{j+1} - l_j) \in \mathbb{R}$. Start with $\rho_{low} = 0, \rho_{upp} = 1$ and then update ρ_{low}, ρ_{upp} according to the rule: if $l_{j+1} > l_j$ set $\rho_{low} \leftarrow \max\{\rho_{low}, q_j\}$. Otherwise set $\rho_{upp} \leftarrow \min\{\rho_{upp}, q_j\}$. If along the computation of the estimates one obtains $\rho_{low} > \rho_{upp}$ we discard y_0, as in the previous cases.
- If all the previous steps have been passed successfully and we reach the Nth iterate, we have y_0 as candidate for $y_{min}(x = 0)$. Then we can decrease the current value of y_0 by some multiple of δ_{y_0} (say, $K\delta_{y_0}$), decrease the current step δ_{y_0} to δ_{y_0}/L for some $1 < L \in \mathbb{N}$ and proceed again. The refinement can be applied several times, but it is not convenient to start with a too large δ_{y_0}. Otherwise we can completely miss zones with "regular" behaviour.

1.2.2 Results and interpretation

Different experiments have been carried out using the previous algorithm. The values used for the different parameters are $N = 2500$, $\delta_{y_0} = 10^{-4}$, $L_{max} = 10^6$, $n = 10$, $S_{max} = 2\sqrt{\alpha + \beta}$, $K = 5$ and $L = 10$. Tests have been made to check the convenience of these choices. Different strategies have been used to save computer time. Most of the time (roughly 98%) is devoted to the computation of iterates under P and DP.

Next figures show different magnitudes in selected regions of the parameter space. In all of them the points on a grid (either 1D or 2D) have been joined with lines, to allow for a more clear representation. Figure 1.1 displays $y_{min}(x = 0)$ for small values of (α, β). It is already clear the staircase structure or, because we are dealing with a surface, a structure of successive cliffs. At each of them there is a jump of $y_{min}(x = 0)$, typically

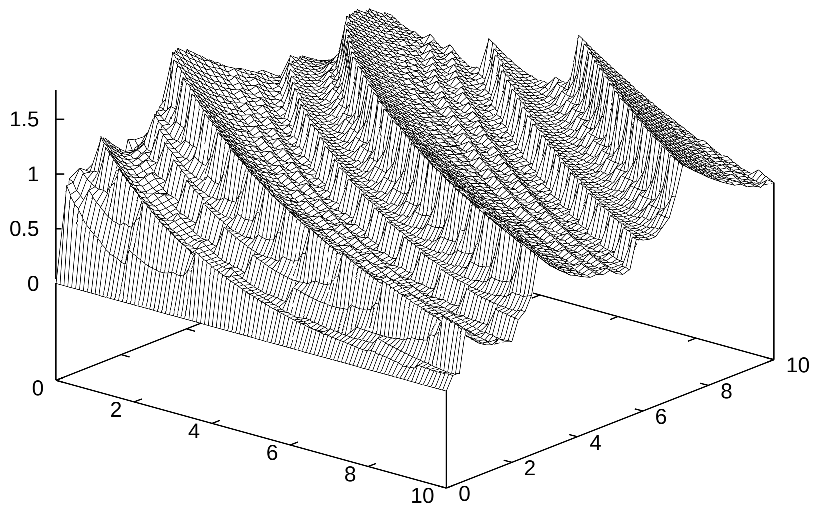

Figure 1.1. Plot of $y_{min}(x = 0)$ for $(\alpha, \beta) \in [0, 10] \times [0, 10]$.

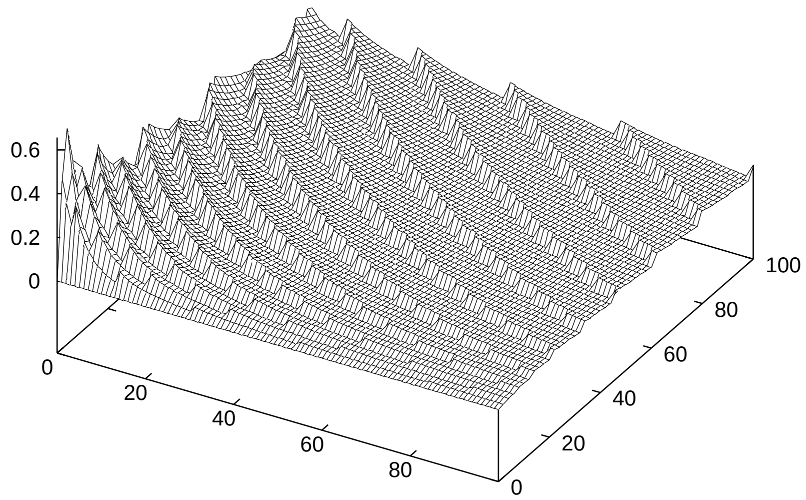

Figure 1.2. Plot of the difference $d(\alpha, \beta) = y_{min}(x = \pi)(\alpha, \beta) - 2\sqrt{\alpha + \beta}$ for $(\alpha, \beta) \in [0, 100] \times [0, 100]$.

followed by a mild decrease. It is interesting to remark that all values of $y_{min}(x=0)$ found, even for large values of (α,β), are below 2.25. Hence, there are *ric* not too far from the origin.

On the other side, an estimate $y_{min}(x=\pi) \simeq 2\sqrt{\alpha+\beta}$ is provided by adiabatic theory. To make the structure apparent we plot the difference $d(\alpha,\beta) = y_{min}(x=\pi)(\alpha,\beta) - 2\sqrt{\alpha+\beta}$ (see figure 1.2). A similar structure appears, with milder cliffs. It is also remarkable that the maximal value of $d(\alpha,\beta)$ is below 0.8.

The plot of $\rho_{y_{min}}$ is more wild, and it is harder to show a clean 3D representation in a single figure. Instead, several sections are shown in figure 1.3, for $\alpha = 0$, 50 and 100. The typical structure is clear: $\rho_{y_{min}}$ increases with β, jumping over every rational value of the image. In same cases there are jumps up and down. When a value more or less close to 1 is reached, a jump to the vicinity of 0 is produced.

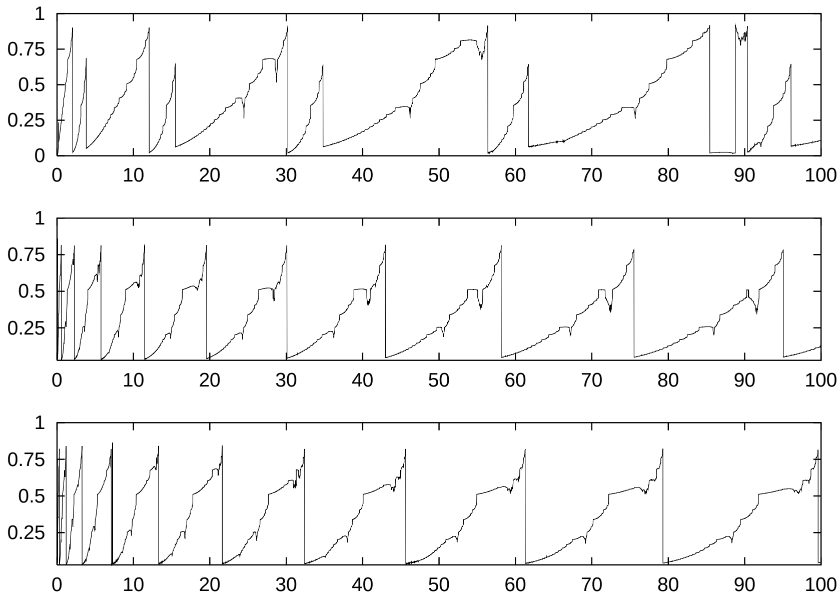

Figure 1.3. Evolution of $\rho_{y_{min}}(\alpha,\beta)$ as a function of β. Top: $\alpha = 0$; centre: $\alpha = 50$; bottom $\alpha = 100$.

The meaning is clear: On the top of the *ric* that we label as y_{min}, there are chains of islands of increasing ρ. Increasing β the *ric* and the islands become closer, the *ric* is broken and the first *ric* that we encounter is on the top of the chain of islands. The process is not monotonous: the dynamics on a vicinity of the island can become smoother and a *ric* can reappear below the chain of islands. This mechanism has been detected in [15]. The possible existence of strips, on (x,y), where the twist character is lost has to be taken into account.

In figure 1.4 we show $y_{min}(x = \pi)$. As said, it essentially behaves like $2\sqrt{\alpha+\beta}$. Only a few upstairs jumps can be seen at this scale (this is the reason to introduce $d(\alpha, \beta)$.) They correspond to the top of the cliffs in figure 1.2 and follow a well defined pattern. It can be seen in the right part of the figure, where we plot points close to $\rho_{y_{min}} = 1$ (in fact places where the values are greater than 0.6 on a rough grid.) These curves correspond to the places where the first *ric* moves from the bottom to the top of an island of period 1. These islands correspond, in the unperturbed pendulum, to circulation orbits with periods of the form $2\pi q$ with $q \in \mathbb{N}$. As an example, for the dots in figure 1.4 (right) very close to (100,100) one has $q = 16$.

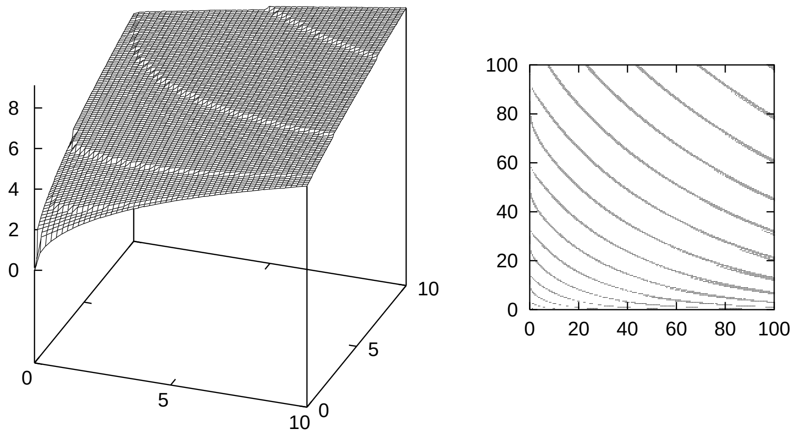

Figure 1.4. Left: the surface $y_{min}(x = \pi)$ as a function of (α, β). Right: points with $\rho_{y_{min}} > 0.6$. Compare with figure 1.2.

1.3 An estimate of the integrability fraction

Next step is to try to figure out the dynamics in DI. We know that for β/α small enough, most of that domain will be filled by invariant curves. What we propose is to have a measure of the "fraction of integrability" inside the domain, in the spirit of the pioneer work [8]. We shall use the Lebesgue measure of the set of points with regular behaviour.

1.3.1 A fast estimate of the chaotic orbits: The algorithm

To produce this estimate we start, for a given (α, β), by recovering the curve y_{min}. Together with $S_x(y_{min})$ they give approximate bounds of the domain. Due to the symmetry it is enough to consider (x, y) in the first quadrant. Then we proceed as follows.

- Find the maximal value, $\hat{y}$, of y_{min}. It occurs at $x = \pi$, except on a very small domain (α, β), $\alpha < 0.008$, bounded by the β axis, a curve $\beta \simeq (2\alpha)^{1/3}$ (where there are equal maxima at $x = 0$ and $x = \pi$) and a curve $\beta = g(\alpha)$, slowly decreasing, with $g(0) \simeq 0.22$ (where a jump to include period–4 islands inside DI occurs).
- Select a value $M \in \mathbb{N}$. This will be the number of pixels we put, in the x and y directions, on the rectangle $[0, \pi] \times [0, \hat{y}]$, having the centres at the points $(\xi_k = k\pi/M, \eta_j = j\hat{y}/M)$ for $k, j = 0, \ldots, M$. For each k we find the maximum index $j(k)$ such that the pixel of label (k, j) is below y_{min}. Hence, the total number of pixels to be scanned is $\sum_{k=0}^{M}(j(k) + 1)$. Note that the area of the pixels with $k = 0$ and $k = M$ should be multiplied by $1/2$, as well as the pixels with $j = 0$.
- Then one takes initial points of the form (ξ_k, η_j) and we proceed to compute iterates under P and also iterates under DP of a random initial vector v_0, $|v_0| = 1$. A maximum of N iterates is computed. The iteration is stopped when either the count N is reached or when the length of $DP^l(\xi_k, \eta_j)v_0$ exceeds some value L_{max}.
- When the iteration is stopped we have decided that the orbit is either regular (0) or chaotic (1). Then all the pixels of the orbit are marked with the character (0 or 1), but a pixel that has been already marked is not marked again. Of course, most of the pixels will contain points of both kinds but, giving prevalence to the first occupancy of the pixel by some point of an orbit, we believe that will reflect, statistically, the dominant character of the pixel. Note that if the iterate $P^l(\xi_k, \eta_j) := (\xi_k^{(l)}, \eta_j^{(l)})$ is not in the first quadrant, the symmetric point $(|\xi_k^{(l)}|, |\eta_j^{(l)})|$ is marked. They have the same character.
- We proceed with the scanning, but skipping all points whose character has already been decided. Finally we count the number of pixels, n_0, n_1, having been assigned the value 0 or 1, respectively. The *fraction of integrability* is defined as *fi* $= n_0/(n_0+n_1)$. We shall use *lfi* to denote log(*fi*).

1.3.2 Results and interpretation

The algorithm has been tested with different values of M, N and L_{max}. Typical values of N and L_{max} are 10^3 and 10^6. No significative differences have been observed by increasing them. For M the values 256 and 512 have been used, depending on the region of the (α, β)–plane explored. The computational effort is proportional to M^2 and higher in regular zones.

Figures 1.5 and 1.6 show the results in the window $[0, 10]^2$, while figures 1.7 and 1.8 correspond to $[0, 100]^2$, with a larger step size. To better visualize the regions where *fi* is small, we have used a logarithmic scale. In both pages the upper figure gives a 3D view and the lower one displays level curves ($\log(fi) \in \mathbb{Z}$) of the upper surface.

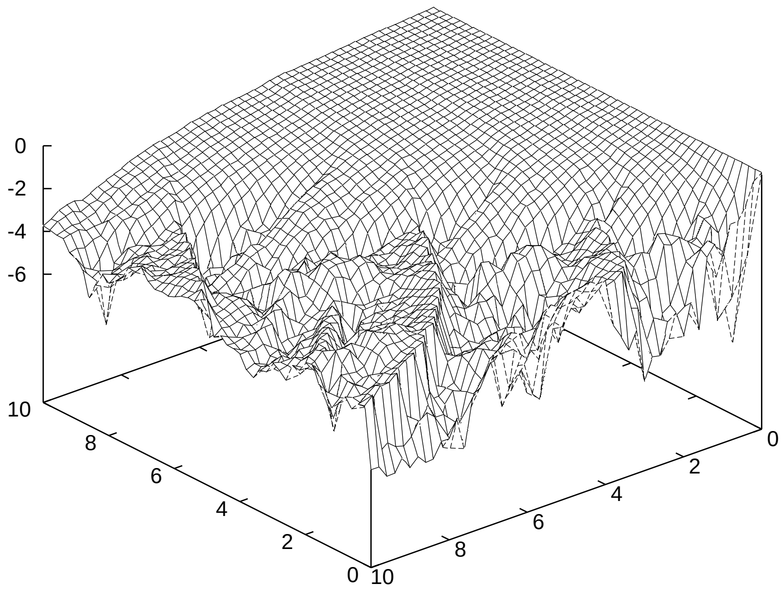

Figure 1.5. Logarithm of the fraction of integrability *lfi* in DI as a function of (α, β).

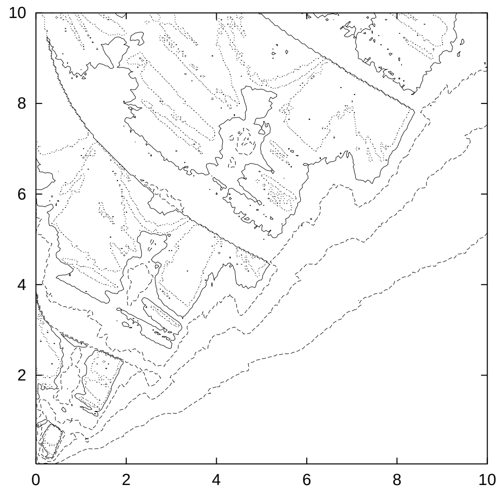

Figure 1.6. Level lines of figure 1.5. Continuous line for $lfi = -4$ broken lines for $lfi = -1, -2, -3$ and dots for $lfi = -5$.

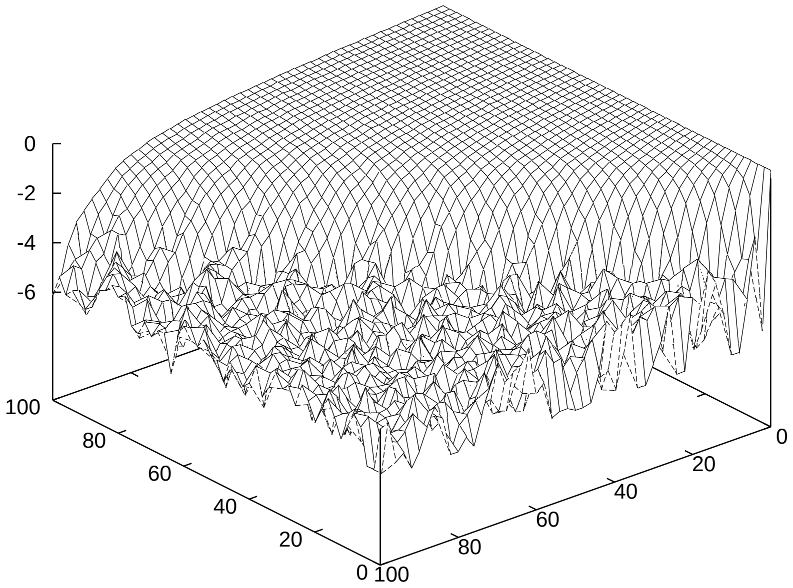

Figure 1.7. Same as figure 1.5 in the domain $[0, 100] \times [0, 100]$.

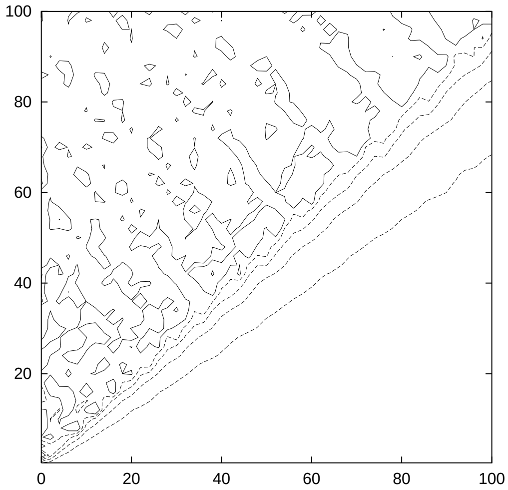

Figure 1.8. Level lines of figure 1.7. Continuous line for $lfi = -5$, broken lines for $lfi = -1, -2, -3, -4$.

As one can expect, for β/α small *fi* is close to one. Fixed a not too small value, say $\mathit{fi} = \exp(-k), i\, k = 1, 2, 3, 4$, it seems that the lines in the (α, β)–plane with this value of *fi* are close to straight lines. However, it looks reasonable to conjecture that all of them become relatively closer to the diagonal, in the parameter plane, when α increases.

Close to the diagonal there is a fast decrease in *fi* and we find, essentially, values below 0.01 . On figure 1.5 is still possible to distinguish the effect of the cliffs of section 1.2.2. They are also clearly seen in figure 1.6, on the solid line of level $\mathit{lfi} = -4$. It is clear that when we move the parameter, so that a relatively large island enters DI, the indicator *fi* increases. Smaller cliffs can be seen on the dotted level curve. Furthermore, close to the line $\beta = \alpha$ some structures are visible, either in figure 1.5 in the form of bumps or in figure 1.6 as oscillations in the line $\mathit{lfi} = -3$.

If we move to figure 1.7 the integrable part is clearly seen, but for $\beta > \alpha$ and not too close to $\alpha = 0$, it is hard to recognize any structure, except the bumps near $\alpha = \beta$ observed in figure 1.6. The levels of *lfi* are small (of the order of -6, i.e., $\mathit{fi} \simeq 1/400$) and the relative error in the determination of *fi* can start to be important. The situation becomes more clear in figure 1.8, where we restrict the levels shown to $\mathit{lfi} \geq -5$ (levels below this one have a more complicate structure to be analyzed in the future). Levels -3 and -4 display oscillations related to the upper bumps. The level $\mathit{lfi} = -5$ (in solid lines) has a pattern of roughly parallel strips.

The origin of the bumps is easily detected. They correspond to the stability regions of the point $(\pi, 0)$. Concerning the strips, if we compare with the location of the cliffs, as shown on the right part of figure 1.4, we see that they are unrelated phenomena.

A possible explanation is as follows. Increasing β, for fixed α, certainly new islands enter DI, the main ones coming from fixed points. As soon as they go inside the chaotic zone they lose stability and do not contribute to *fi* . Furthermore, the relative width of these islands, compared to the size of DI, becomes smaller when β increases. Indeed, the islands become thinner and, at the same time, the area of DI increases.

But inside DI other islands appear, mainly around fixed and period–2 points on the x axis, on $x = \pi$ and, with less importance, on $x = 0$. Just to cite a few of them, on the x axis there appear systematically (i.e., along families of curves in the (α, β)–plane) islands near $x = 0.25$, 0.5, 0.85, 1.2, 1.5, 1.85, 2.2 and 2.6 . The most relevant ones are located close to 0.5 and 2.6. When they appear they have a relatively large contribution to *fi* .

This is illustrated in figure 1.9, where *lfi* is plotted, with a small step size, for $\alpha = 0$, 50 and β ranging from 0 to 100. For convenience we display on the same plots the function $y_{min}(x = 0)(\alpha, \beta)$ (shifted vertically and magnified to use the same scale) for the same values of α. While in the upper figure there is a good agreement between cliffs of this last function and sudden increases of *lfi*, in the lower one there are many other bumps of *lfi* unrelated to the jumps of $y_{min}(x=0)$.

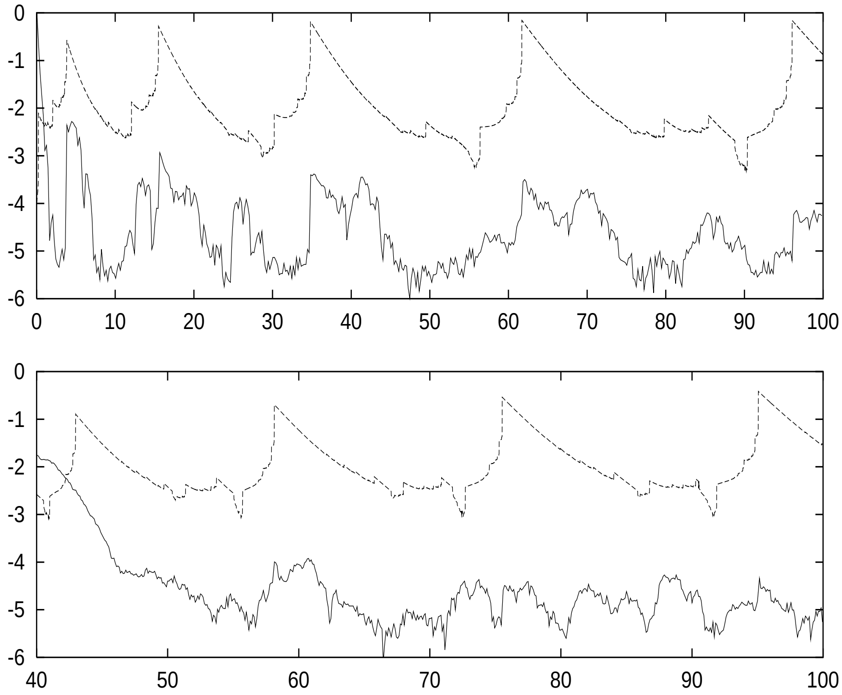

Figure 1.9. Graphs of *lfi* as a function of β. Top: $\alpha=0$; bottom: $\alpha=50$. For comparison purposes we also plot $2y_{min}(x=0)-4+\alpha/100$. See text.

Furthermore is must be added that the different (major) islands contributing to *fi* have a changing importance when they are continuated with respect to α and β. Assume, for definiteness, that we follow some path on the (α,β)–plane. Assume also that, following that path we find a *centre–saddle* bifurcation, where the elliptic periodic point is born, and later we find a period doubling, so that the trace, Tr, of DP^k (if the period is k) decreases monotonically from 2 to -2. Then we can ask for the behaviour of the size of the island around the periodic point. Generically it will be zero when $\mathrm{Tr}=-1$, the eigenvalues being cubic roots of the unity, and a local minimum appears when $\mathrm{Tr}=0$, when the eigenvalues are $\pm i$. A remarkable thing (tested in different examples, see [15]) is that the maximum area of the island seems to occur when the rotation number of the last invariant curve around the periodic point is between 1/10 and 1/9.

1.4 A model problem in $2\frac{1}{2}$ degrees of freedom

Finally we come to a problem in higher dimension. Consider the Hamiltonian

$$\begin{aligned} H(y,I_2,I_3,x,\theta_2,\theta_3) = {} & \frac{1}{2}(y^2+I_2^2)+I_3 \\ & +\varepsilon(\cos x-1)\,(1+\mu(\cos\theta_2+\cos\theta_3))\,. \end{aligned} \quad (1.2)$$

This is the classical Arnol'd example of diffusion [1], but we shall consider both parameters, ε and μ, as equal. This is a difficult problem, because the splitting estimates of (1.2) given in [1] strongly rely on the fact that μ can be taken exponentially small with respect to ε. Here the unperturbed Hamiltonian contains the terms of degrees 0 and 1 in ε, while the terms in ε^2 are the perturbation. Furthermore, the entire character of the perturbation $(\cos x-1)(\cos\theta_2+\cos\theta_3)$ adds more difficulties, because the splitting of the separatrices of the hyperbolic tori ($x=y=0$, I_2 fixed and $(\theta_2,\theta_3)\in\mathbb{T}^2$), becomes much smaller than in a general analytic case. See [17] and [16] for motivation and several results.

Assume we are interested in the vicinity of $I_2=\omega$. Scaling and shifting variables and time and introducing $\eta=\sqrt{\varepsilon}$ we obtain the system

$$\begin{aligned} y' &= \eta x\,, \\ J_2' &= \eta^3(\cos x-1)\sin\theta_2\,, \\ x' &= (\eta+\eta^3(\cos\theta_2+\cos\theta_3))\sin x\,, \\ \theta_2' &= \omega+\eta J_2\,, \\ \theta_3' &= 1. \end{aligned} \quad (1.3)$$

We want to have an idea of the global properties of (1.3). We can start at the Poincaré section $x=\pi$, select $J_2=0$ (this is irrelevant because we can change ω) and take as parameters the initial value of y and ω. The only restriction we impose is that we take the initial value of $\theta_3(=t)$ as zero.

1.5 Computation of the local exponential growth of the distance

To decide about the domain of regular and chaotic dynamics for system (1.3) it can be enough to use the method proposed in section 1.2.1. However, we shall use a different one, which allows also to obtain the maximal Lyapunov exponent, Λ. To compute a numeric approximation to Λ it is enough (with probability 1) to take an arbitrary vector v and transport it by the variational flow. Let $v(t)$ be the vector obtained. Then the expression $\log|v(T)|/T$, for an increasing sequence of values of T, provides approximations to Λ. Several problems can occur.

- The orbit used to transport v enters different regions where the local rate of divergence of nearby orbits is very different. This would suggest not to take values of T too large. One of the typical unpleasant problems, in this context, is that the orbit can spend long periods of time, in a quasi-random way, close to invariant objects (invariant curves or tori, known to be sticky). Then the estimates of Λ can seem to converge to zero for a while.
- Nearby orbits diverge in a regular way, but they have periodic or quasi-periodic oscillations added (or multiplied) by the exponential growth. Even in simple systems (e.g., in the linear case, cf. [4]) this can slow down the method. One has to take care about the location of the orbit at the end of the time intervals used to estimate Λ.
- It is convenient to use some average or smoothing of the data, or to replace them by some "envelope", which will converge to the correct value much faster. It is also more suitable for extrapolation. See [4] for details.

Recently an averaging method has been proposed [7]. It supplies an indicator of the regular or chaotic behaviour and produces estimates of Λ.

1.5.1 The method

As described in [7] we introduce an indicator of the mean exponential growth factor of nearby orbits (MEGNO). Let us consider a differential equation $x'(t) = f(t, x(t))$ and the associated variational flow $v'(t) = D_x f(t, x(t))v(t)$, starting at an initial point x_0 with a random vector v_0. Then we can define the auxiliary differential equations

$$y' = t(v, v')/(v, v), \quad z' = 2y/(1+t). \tag{1.4}$$

It is clear that for regular orbits, with a linear rate of separation of nearby orbits, the quotient $2y(t)/t$ converges to 2 when $t \to \infty$. On the other side for orbits (and initial vectors) having a maximal Lyapunov exponent Λ, it diverges as Λt. The variable z is smoothing these quotients. Hence $w(t) := z(t)/t$ also tends to 2 for regular orbits (except in the non-generic cases of super-linear separation) and behaves as $\Lambda t/2$ in the chaotic case. Let T be the final time used in a computation and let $t_j = jH$, $j = j_0, \ldots, m$, where $H = T/m$ is some moderate time step and j_0 accounts for a transient to be skipped. The sequence of values $\{w(t_j)\}$ can be fitted by a line. The slope produces an estimate of $\Lambda/2$.

Either with this estimate or simply with the values of $w(T)$ at some final time, one can devise a method to detect the character of a given orbit. Equations (1.4) must be integrated simultaneously with the field equations, in our case (1.3), and the corresponding first variationals.

1.5.2 Description of results

The method described in section 1.5.1 has been applied to (1.3) for a sample of $\eta \in [0.1, 0.3]$. In figure 1.10 a result is presented. It corresponds to $\varepsilon = 0.0625$ ($\eta = 0.25$). The algorithm has been applied to an equispaced grid of 2000×2000 pixels in the domain $(y, \omega) \in [0, 5] \times [0, 2]$. The initial values of the remaining variables have been given above. The value $T = 10^4$ has been used. Orbits such that $w(T) < 1.92$ have been selected as regular, while orbits with $w(T) > 2.08$ are considered chaotic. The intermediate range is considered as, possibly, mildly chaotic. The values have been selected to have a good contrast between both kinds of orbits.

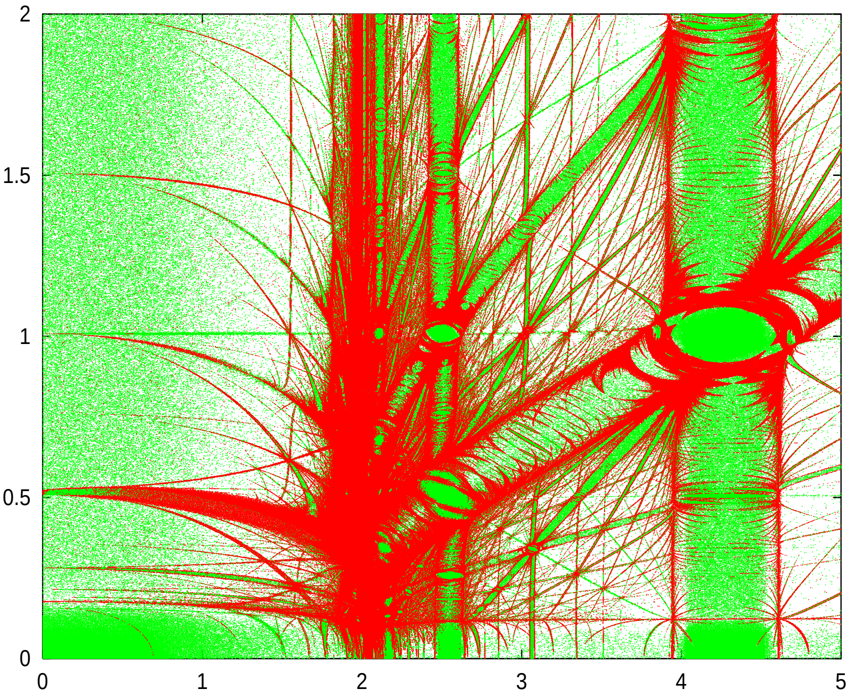

Figure 1.10. Regions of regular motion (light grey) and chaotic motion (dark grey). The horizontal (resp. vertical) axis corresponds to the y variable of the pendulum (resp. the initial frequency, ω, of the angle θ_2.)

In figure 1.10 the pixels corresponding to initial conditions of regular type (resp. with chaotic behaviour) have been plotted in light grey (resp. dark grey). Let us describe the meaning of what we can observe in figure 1.10. A resonance can be identified as a light grey channel surrounded by dark grey boundaries. If it is very thin perhaps some trace of the light grey and/or dark grey can be seen. Hundreds of resonances can be detected in figure 1.10.

In the unperturbed case (i.e., if be delete only the terms in η^3 in (1.3)) $y = 0$ (resp. $0 < y < 2$, $y = 2$, $y > 2$) corresponds to the elliptic fixed point (resp. the libration orbits, the separatrix, the circulation orbits) of the pendulum part. We recall that the section has been taken on $x = \pi$. The "external" frequencies are now ω and 1. The resonances occur for the pendulum periodic orbits (either of libration or circulation type) whose frequency $\nu(y,\eta)$ satisfies $k_1\nu + k_2\omega + k_3 = 0$, $k_1, k_2, k_3 \in \mathbb{Z}$. All of them have zero width and are located on horizontal lines (if $k_1 = 0$), on vertical lines (if $k_2 = 0$) and on a countable set of curves $\omega = (-1/k_2)(k_1\nu + k_3)$, otherwise. We recall that $\nu(y,\eta) \to 0$ as $y \to 2$. This explains the general pattern of the resonances.

To recover the perturbed problem of (1.3) we can replace the η^3 factor by $\eta\gamma$ and let γ move from 0 to η^2. This is quite different to change η in (1.3), because in this last case the frequency $\nu(y,\eta)$ also changes.

The "centre line" of each resonance channel corresponds to 2D (normally) elliptic tori, while the "boundary lines" corresponds to 2D hyperbolic tori. When two resonances cross there is a periodic orbit at the "centre" of the crossing. If the centre of the crossing is seen as a zone of regular motion the periodic orbit is of totally elliptic type. Generically the light grey regions correspond to 3D tori. Note that the chaotic regions seem to be connected. This gives the possibility to have diffusion, but figure 1.10 tells us nothing about in which direction the instability takes place and with which probability. A detailed geometric study is required to check the heteroclinic connections. Alternative efficient indicators of the quantitative details of the diffusion are also desirable. Both aspects are works in progress.

1.6 Conclusion

Several tools have been presented to give detailed indications on the global dynamics of different systems. Many other are available, like the well known frequency analysis. Combination of different tools can give (relatively) fast and reliable methods to guess the main features of the dynamics and their significance. In this paper it has been demonstrated the efficiency of the fast indicators.

Acknowledgements

I would like to express my gratitude to H Broer, P Cincotta, A Jorba, M van Noort, T Stuchi, D Treschev and C Valls, who have largely contributed to this paper, by means of discussions, suggestions and/or questions. The work has been supported by grants BFM2000–805 (Spain), 2000SGR–27 (Catalonia) and INTAS 97–771. The computing facilities of the UB–UPC Group of Dynamical Systems have been used.

References

[1] Arnol'd V I 1964 *Sov. Math.,Dokl.* **5** 581

[2] Broer H, Hoveijn, van Noort M, Simó C and Vegter G 2001 "Global coherent dynamics of the parametrically forced pendulum: a case study in $1\frac{1}{2}$ degrees of freedom" Preprint

[3] Broer H, Roussarie R and Simó C 1996 *Ergod. Th. & Dynam. Sys.* **16** 1147

[4] Broer H and Simó C 1998 *Bul. Soc. Bras. Mat.* **29** 253

[5] Broer H, Simó C and Tatjer J C 1998 *Nonlinearity* **11** 667

[6] Cincotta P and Simó C 1999 *Cel. Mechanics & Dynam. Astron.* **73** 195

[7] Cincotta P and Simó C 2000 *Astron. & Astroph. Supp.* **147** 205

[8] Hénon M and Heiles C 1964 *Astron. J* **69** 73

[9] Ivanov A 2000 *Regular & Chaotic Dynamics* **5** 329

[10] Jorba À and Zou M 2001 "On the numerical integration of ODE by means of high-order Taylor methods" Preprint

[11] van Noort M 2001 "The parametrically forced pendulum. A case study in $1\frac{1}{2}$ degrees of freedom" Ph. D. Thesis Univ. Groningen

[12] Simó C 2001 "Dynamical properties of the figure eight solution of the three-body problem" Preprint

[13] Simó C, Broer H and Roussarie R 1991 *Proc. European Conf. on Iteration Theory, Batschuns* (Singapore, World Scientific) p 320

[14] Simó C and Stuchi T 2000 it Physica D **140** 1

[15] Simó C and Treschev D 2000 "Evolution of the "last" invariant curve in a family of area preserving maps: The case of the separatrix map" Preprint

[16] Simó C and Valls C 2000 "A formal approximation of the splitting of separatrices in the classical Arnold's example of diffusion with two equal parameters" Preprint

[17] Valls C 1999 "The classical Arnold example of diffusion with two equal parameters" Ph. D. Thesis Univ. Barcelona

Appendix

Consider a dynamical system given by a differential equation

$$x' = f(t, x)\,. \tag{1.5}$$

We look for the representation of the solution of (1.5) around some given initial conditions (t_n, x_n) as $x(t_n + h) = \sum_{k=0}^{n} x^{(k)} h^k$. This expansion will be truncated at a suitable order, to be discussed later.

We can assume, with full generality, that the components of f can be expressed as the composition of arithmetic $(+, -, *, /)$ operations and elementary functions (basically $\log, \exp, \sin, \cos$). If the representations of two functions $q(t), p(t)$ are known to order k, it is immediate to write the representation of $p \bullet q$, where $\bullet$ denotes any of $+, -, *, /$. To obtain the new truncated series to order N the cost is $O(N^2)$. The same applies to obtain $p = \log q$ from the relation $p'q = q'$, $p = \exp q$ from $p' = pq'$ and

$p = \cos r$, $q = \sin r$ from $p' = -qr'$, $q' = pr'$. Again the cost is $O(N^2)$. Note that we should work with numerical (non-literal) coefficients.

Routines to produce the jet to order N, if a code producing the evaluation of $f(t,x)$ from t and x is available, are easy to write. For one of such implementations we refer to [10].

A key point is the selection of the suitable order N and the variable time step h. To this end we must assume analyticity and some "good" behaviour of the Taylor series.

Proposition 1. Let $\rho = \rho(t)$ be the radius of convergence around the point (t_n, x_n). Assume the coefficients $x^{(k)}$, in the Taylor representation of the solution, satisfy $A_1\rho^{-k} < |x^{(k)}| < A_2\rho^{-k}$ for some $0 < A_1 < A_2$. Then, to obtain a prefixed relative error in each step the more efficient step size (in the computational sense) tends to $h = \rho/\exp(2)$ when the error tends to zero.

Remark 1. In cases where the assumption is obviously false (e.g. the series contains only odd terms) one can modify in a suitable way with the same result. The value of $\rho(t)$ can be estimated from the behaviour of the coefficients $x^{(k)}$.

Proof of proposition 1 Assume we want a relative error at most ε in each step (this can be the ε of the computer or, eventually, the adopted multi-precision value). Let $\hat{h} = h/\rho$. Except by a constant factor it is enough to take $\hat{h}^N = \varepsilon$. For fixed ε this gives a constrain for h and N. On the other hand the cost per unit of t is $C \simeq h^{-1}BN^2$, where we use the $O(N^2)$ character of the method. Minimizing C under the constrain, if ε is small enough, leads to maximize $(\log \hat{h})^2/\hat{h}$. From this the result follows. Note that the effects of the quotient A_2/A_1 and of the terms of order $> N+1$ can be bounded by a constant, independent of ε, and become negligible if $\varepsilon \to 0$. □

The method is specially interesting if ε is small (e.g., integration in multi-precision, say $\varepsilon = 10^{-34}$.) In principle the only errors it produces are the unavoidable rounding errors. However it can lose efficiency in two cases:

(i) The evaluation of f requires a big amount of operations.
(ii) Along the orbit one passes close to some singularity (i.e., ρ becomes very small). This singularity can be located at some complex t.

From proposition 1 follows that the value of N is, essentially, $-\frac{1}{2}\log\varepsilon$. For a typical value $\varepsilon = 10^{-16}$ an order around N=18 is suitable. Note that as this ε can be not small enough, some slightly different orders can have a better performance.